THE JOURNAL OF PHYSICAL CHEMISTRY B

Article

pubs.acs.org/JPCB

Creation and Persistence of Chiral Asymmetry in a Microscopically Reversible Molecular Model

Francesco Ricci,[†] Frank H. Stillinger,[‡] and Pablo G. Debenedetti*,[†]

[†]Department of Chemical and Biological Engineering and [‡]Department of Chemistry, Princeton University, Princeton, New Jersey 08544, United States

ABSTRACT: Of the numerous mechanisms that have been postulated to explain the origin of biological homochirality, asymmetric autocatalysis coupled with mutual inhibition is often cited as a plausible route to abiotic symmetry breaking. However, in a system closed to mass flow, the constraint of microscopic reversibility ensures that this far-from-equilibrium phenomenon can at best provide a temporary excursion from racemic equilibrium. Comparatively little attention has been paid in the literature to the manner in which such a closed system approaches equilibrium, examining the mechanisms and time scales involved in its transit. We use an elementary lattice model with molecular degrees of freedom, and satisfying microscopic reversibility, to investigate the temporal evolution of stochastic symmetry breaking in a closed system. Numerical investigation of the model's behavior identified conditions under which the system's evolution toward racemic equilibrium becomes extremely slow, allowing for long-time persistence of a symmetry-broken state. Strong mutual inhibition between enantiomers facilitates a "monomer purification" mechanism, in which molecules of the minor enantiomer are rapidly sequestered and a nearly homochiral state persists for long times, even in the presence of significant reverse reaction rates. Simple order of magnitude estimates show that with reasonable physical parameters a symmetry-broken state could persist over geologically relevant time scales.

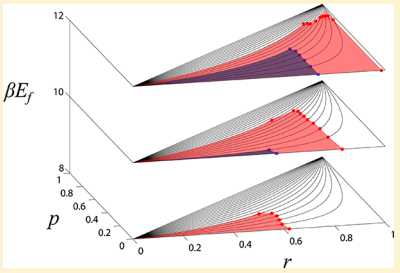

I. INTRODUCTION

The chemistry of life is overwhelmingly homochiral. For example, the 19 naturally occurring chiral proteinogenic amino acids are found overwhelmingly as L-enantiomers in living organisms, while most naturally occurring sugars are found in the D-form (such as the ribose sugars found in DNA). A recent study[1] has shown that, of the 187 941 074 recorded amino acid sites in the proteome, a mere 837 (that is, 4.5 per 1 million sites) are D-isomers. In light of such statistics it is clear that homochirality is a signature of life as we know it, and natural questions arise regarding its origins.

While there is no general consensus among researchers regarding the origin of biological homochirality, it is not for lack of hypotheses. A common thread shared by many proposed scenarios is that the prebiotic world was presumably racemic. Therefore, this viewpoint stresses the importance of chiral symmetry breaking events giving rise to enantiomeric excess of simple molecular building blocks, leading eventually to more complex enantiopure molecules and, in due course, to homochiral life. It is generally assumed that the path from abiotic chiral symmetry breaking to homochiral life requires three essential occurrences: the creation of an initial, likely slight, imbalance in the enantiomeric excess of a chiral species; the accompaniment of that imbalance with an amplification mechanism capable of producing macroscopic symmetry breaking; and the maintenance of the symmetry-broken state over time scales necessary for chemistry and evolution to eventually give rise to homochiral life as we know it.

Several mechanisms for the origin of biological homochirality have been postulated, and many have been experimentally observed in the laboratory. A broad classification of these mechanisms stresses their stochastic or deterministic character. Stochastic theories of symmetry breaking imply that the currently observed preponderance of L-amino acid and/or D-sugars occurred by chance, meaning that life might have just as easily formed with, for instance, D-amino acids and L-sugars. Among the several hypothesized stochastic mechanisms for the origin of biological homochirality, a general distinction may be made between physical and chemical mechanisms. One notable physical mechanism for the amplification of an initially small enantiomeric imbalance is thermodynamic phase equilibrium enantioenrichment.[2−5] This phenomenon pertains to fluid−solid phase equilibrium between racemic and enantiopure crystals, and an achiral solvent in which the solubility of the enantiopure crystal is greater than that of the racemic crystal. For systems exhibiting this phase behavior, a slight initial enantiomeric imbalance may become greatly amplified in the liquid phase at equilibrium. This property has been exploited through the addition of additives that enhance the stability (hence low solubility) of the racemic crystal,[6,7] leading to increased liquid-phase enantiomeric excess.

Physical mechanisms for solid-phase stochastic symmetry breaking have also been studied. For example, significant solid-phase symmetry breaking has been observed during the crystallization of an achiral salt that forms chiral crystals.[8−10] With sufficient stirring during the crystallization, the newly

Received: September 20, 2012
Revised: December 17, 2012
Published: December 19, 2012

   dx.doi.org/10.1021/jp3093644 | J. Phys. Chem. B 2013, 117, 602−614

formed crystal population exhibits a high level of enantiomeric excess, while in the absence of stirring a racemic mixture of crystals is produced. This phenomenon has been demonstrated for explicitly chiral molecules which form conglomerate (enantiopure) crystals as well.[11] Another interesting mechanism which produces random solid-phase symmetry breaking in the absence of an initially imposed chiral bias has been termed "Viedma ripening".[12−17] This phenomenon pertains to a system that has already reached solid−liquid equilibrium involving conglomerate crystals. Upon continued abrasive grinding of this slurry, a completely homochiral state is obtained in the crystal population, even when the initial crystal distribution is nearly racemic.

Perhaps the most widely cited chemical mechanism for stochastic symmetry breaking involves chiral autocatalysis and mutual inhibition. This mechanism was first articulated in 1953 when Frank[18] proposed a set of differential equations describing the amplification of an initial enantiomeric imbalance. This amplification is caused by an irreversible autocatalytic reaction mechanism coupled with mutual inhibition between competing enantiomers.

Given their prominent role in biology, several theories and experimental studies have also examined the formation of homochiral polymers.[19−22] Along these lines, many have studied solid-solution adsorption/polymerization interactions. For instance, oligomerization of racemic mononucleotides on montmorillonite clay (formed by the weathering of volcanic ash) exhibits a homochiral selectivity which preferentially produces homogeneous D- and L-ogliomers.[23−25] This mechanism may help to explain how homochiral polymeric precursors to RNA could have formed in the prebiotic world.

In contrast to stochastic hypotheses, deterministic hypotheses for the origin of biological homochirality assert that life as we know it was predestined to be composed of L-amino acids and D-sugars. A well-studied deterministic hypothesis involves quantum mechanical parity violating forces.[26−30] According to this hypothesis, miniscule energy differences of quantum mechanical origin exist between enantiomers and are responsible for the inevitable preference toward L-amino acids and D-sugars. While several theoretical studies of this phenomenon exist, to date there has been no compelling experimental evidence to support the deterministic viewpoint.[31]

One may note that there is sometimes significant overlap in many of the aforementioned hypotheses of mechanisms for the origin of biological homochirality. For example, certain models of homochirality resulting from polymerization processes invoke autocatalysis and mutual inhibition as postulated by the Frank model,[18] which describes chemical reactions in a nonpolymerizing system.[22,32,33] As another example, some have examined mathematically deterministic systems in which parity violating forces are coupled to a chemical amplification mechanism such as that proposed in the Frank model.[28,34] Among the most recent studies, it has been observed that chemical and physical processes may be coupled, allowing an enantioenriched pool of amino acids to cause the enantioenrichment of a pool of sugars, or vice versa.[35] Excellent reviews on the aforementioned theories may be found in the literature.[31,36]

Some 40 years after its formulation, the first experimental realization of the Frank model was discovered by Soai et al.[37−40] As is the case with many laboratory experiments, the Soai reaction is typically performed in systems closed to mass flow. The principle of microscopic reversibility[41] ensures that the equilibrium state for such a reaction system contains a racemic mixture of enantiomers.[42,43] Thus, in a closed system, the macroscopic amplification of any small enantiomeric imbalance is not permanent and should eventually decay to the racemic equilibrium state by way of the reverse reaction mechanisms. The chiral symmetry breaking created by such a kinetic mechanism is therefore considered a "far-from-equilibrium" phenomenon.[31] All chemical reactions being reversible to some degree, a natural question therefore arises as to how long an imbalance in enantiomeric excess can be preserved, given small but nonzero reverse reaction rates.

It has been shown that variants of the original Frank model that include reversible reactions in a well-mixed open system, analogous to a continuous-stirred tank reactor (CSTR),[44] may be operated at nonequilibrium steady states that are symmetry-broken when the product of reactant concentrations exceeds a critical value.[28,34,42] At this critical value the system bifurcates away from the stable racemic steady state, and at larger values of reactant concentration the resulting stable states are increasingly symmetry broken. Hence, under certain conditions, kinetics allows a well-mixed macroscopic flow system to persist indefinitely in a far-from-equilibrium (nonracemic) steady state. In the prebiotic world, one might envision scenarios reminiscent of a CSTR (perhaps a rock crevice located near the flow field of a thermal vent); however, it is also quite reasonable to envision an alternative scenario without continuous flow or steady state character, such as a pond. Indeed, Darwin's "warm little pond"[45] might have behaved much more like a closed system with only intermittent addition or removal of material. Therefore, it is of considerable interest to determine how such kinetic mechanisms fare in the absence of continuous feeding of reactants and removal of products.

As mentioned above, thermally activated reactions performed in a closed system obey microscopic reversibility, and as a result the system inexorably achieves the racemic equilibrium state after the requisite equilibration time. In spite of this, some researchers have suggested that the inclusion of reverse reactions can help the closed system achieve a stable symmetry-broken state by allowing for the minor enantiomer to become consumed or "recycled" and converted to the major enantiomer.[46,47] However, it was readily shown that either the proposed mechanisms or the chosen reaction parameters in these models were inconsistent with the principle of microscopic reversibility.[43,48] It has therefore been concluded that thermally activated chiral reactions in a closed system can at most achieve a quasi-steady nonequilibrium state which will eventually become racemic.[49,50]

Soai-type reactions and any of their still undiscovered biochemically relevant analogues may produce and maintain appreciable symmetry breaking on laboratory time scales, but for how long can this enantiomeric excess persist in a system closed to mass flow? Equally important, how do such systems behave as the chiral asymmetry decays to racemic? In a prebiotic scenario, such considerations would be of relevance to a far-from-equilibrium mechanism. Yet, to our knowledge, this question has not received explicit attention in the literature.

Most of the modeling performed in the field of chiral symmetry breaking implicitly assumes the validity of mass action kinetics, which is generally only a valid approximation in the limit of a well-mixed system. Hatch et al.[51] recently investigated an elementary lattice model containing microscopic degrees of freedom and explicitly chiral entities. In this model, prochiral reactant species are able to react irreversibly,

dx.doi.org/10.1021/jp3093644 | J. Phys. Chem. B 2013, 117, 602−614

forming chiral products that may then autocatalyze production of their own enantiomer, or mutually inhibit the opposite enantiomer. These authors were able to demonstrate the occurrence of a symmetry breaking transition and to map the region of parameter space where it occurs.

A limitation of the Hatch et al. model[51] is that the enantiomer-forming reactions are irreversible. In this work, we extend the model of Hatch et al., thereby combining microscopic degrees of freedom, explicitly chiral entities, and microscopic reversibility. We explore the spontaneous generation, amplification, and preservation of chiral asymmetry for arbitrarily long times, as mediated by the reverse rates of reaction and other pertinent system variables. It is demonstrated that strong mutual inhibition not only improves the extent of symmetry breaking and the parameter space over which symmetry breaking is realized, but it can also significantly lengthen the time scales over which symmetry breaking persists—even with appreciable reverse reaction rates. Furthermore, it is shown that strong mutual inhibition can provide a mechanism for the maintenance of a nearly enantiopure population of chiral monomers over very long times. Temperature effects are also explored.

This paper is structured as follows. In section II, we describe the model and the numerical methods by which it is investigated. Section III provides an overview of the model's parameter space. In section IV, the results are presented and discussed. In section V, we provide order of magnitude arguments to investigate the implications of the observed results for the origin of biological homochirality. Finally, in section VI concluding remarks are provided along with future directions for research.

II. MODEL AND NUMERICAL METHODS

In our model the achiral reactant species (A and B_2) diffuse on a two-dimensional (2-D) square lattice by rotation or through nearest-neighbor jumps. Multiple occupancy of a lattice site is not allowed, and unoccupied lattice sites may be viewed as either consisting of void space or being occupied by an implicit, chemically inert solvent. Referring to Figure 1a, when A and B_2 come into contact with each other in the correct mutual orientation, they can attempt a reaction according to a thermally excited acceptance probability $\exp(-\beta E_f)$, where $\beta = 1/k_B T$, k_B is Boltzmann's constant, T is the absolute temperature, and E_f is the energy of activation for the forward reaction ($E_f \geq 0$). If the reaction is accepted, A and B_2 bind together to form a chiral product, C, which is of handedness "*R*" or "*S*" depending on its geometry. Note that C forms two nonsuperimposable mirror images in two dimensions; hence these are chiral objects. We use the *R*/*S* nomenclature for the chirality of a molecule, as suggested by IUPAC.[52] Figure 1b illustrates the autocatalytic reaction: should an A and B_2 fall by random diffusion into the cleft of a C molecule, with A and B_2 having the *same* chiral orientation as the existing C molecule, then an autocatalytic reaction is possible. If selected, the autocatalytic reaction occurs with probability $\exp(-\beta E_f^{cat})$, where E_f^{cat} is the autocatalytic activation energy, subject to $0 \leq E_f^{cat} \leq E_f$. Lastly, Figure 1c illustrates heterochiral inhibition between chiral molecules: if two C molecules of opposite chirality diffuse into a configuration in which they fill each other's clefts, a mutually inhibiting physical association is possible, yielding a heterochiral dimer complex. We choose to label the heterochiral dimers "D", in order to differentiate between the populations of chiral molecules which are uninhibited (monomers) vs inhibited (dimerized). If selected, the dimerization occurs with probability 1.

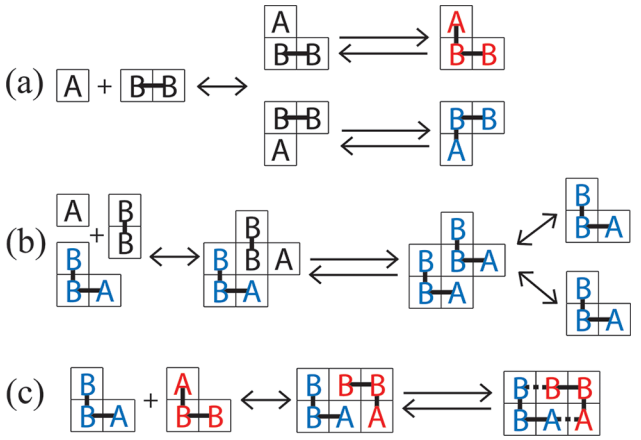

Figure 1. Possible chemical interactions in the model, with "↔" denoting a diffusive move, "→" and "←" denoting chemical reactions, and "—" denoting a chemical bond. The chemical interactions are (a) noncatalytic reaction, (b) autocatalytic reaction, and (c) mutual inhibition mechanism, also referred to as "dimerization" or "heteroinhibition". The mutual inhibition step may be thought of as a physical association; hence the dotted bond lines represent an associative interaction of strength ε.

As indicated in Figure 1, all of the aforementioned reactions can occur in reverse according to their respective Boltzmann factors which are not all independent, as will be explained shortly. If selected, reverse noncatalytic and autocatalytic reactions in Figure 1 may occur with probabilities $\exp(-\beta E_r)$ and $\exp(-\beta E_r^{cat})$, subject to $0 \leq E_r^{cat} \leq E_r$. The dissociation of the mutually inhibiting dimer may occur with probability $\exp(-\beta\varepsilon)$, where ε is the dimer binding energy, subject to $0 \leq \varepsilon < \infty$. Further details on the model are provided in the Appendix.

The simulations are implemented with a kinetic Monte Carlo algorithm[53,54] using simple rejection for diffusive transitions and thermal excitation for reactive/associative transitions. Simulations are performed on an n-by-n square lattice. Each lattice site is of length and width l, and periodic boundary conditions are employed. The coverage fraction due to occupied sites on the lattice is denoted by the symbol φ.

The simulations begin with an equimolar mixture of A and B_2 at the designated coverage fraction. As was done by Hatch et al.,[51] the particles are initially arranged in a symmetrical configuration with no bias toward the production of one enantiomer over the other. There is an initial "mixing" period of 10 000 Monte Carlo (MC) steps, during which the particles are only allowed to randomly diffuse. After this mixing period, reactions are also allowed to occur.

In each MC step a particle is randomly selected and the simulation time is advanced by $(1/N)\tau$, where N is the total number of particles at that point in time, and τ is the unit of simulation time, formally defined as the average time over which each particle is visited once by an implicit heat bath.[53,54] After the initial mixing period, diffusive or reactive moves are attempted with equal probability on a randomly chosen particle. If a diffusive move is selected, the particle is chosen to either translate or rotate, with the directionality also chosen randomly. If the required nearest-neighbor sites are unoccupied, the translation/rotation is accepted. If the particle is selected for reaction, the algorithm detects whether that particle

dx.doi.org/10.1021/jp3093644 | J. Phys. Chem. B 2013, 117, 602−614

is in the correct configuration to undergo any of its possible reactions (i.e., an A particle can only react with a B_2 in the correct configuration to form a C via noncatalytic or autocatalytic routes). If one or more reactions are possible at that moment, one of them is chosen randomly and the reaction probability (Boltzmann factor) is then compared with a pseudorandom number $\in [0, 1)$ as a test for acceptance.

The characteristic time scale for diffusion is determined on the basis of the measured diffusivities of species A, B_2, and C on the lattice as a function of composition (see the Appendix for more detail). The diffusion time for species i is calculated as

$$t_{d,i} = \frac{(nl)^2}{D_i} \tag{1}$$

where n = system lateral size, l = width of a lattice site, and D_i = diffusivity of species i in units $[l^2/\tau]$. Without inhibition ($\varepsilon = 0$), the diffusion time of reactant species B_2 is used as a measure of the characteristic diffusion time. However, in the presence of strong inhibition ($\varepsilon/E_f \geq 1$), the formation of product dimers becomes a major contributor to the lengthening of the time required to achieve equilibrium. Therefore, when $\varepsilon/E_f \geq 1$ the diffusion time of species C is used as a measure of the characteristic diffusion time. Intermediate values of ε/E_f in the range $0 < \varepsilon/E_f < 1$ exhibit relatively weak inhibition. Such values were also briefly explored, but are not presented in this paper. The characteristic time for reaction (t_r) was chosen as the reaction half-life with respect to species A. When the characteristic diffusion (reaction) time is greater than the characteristic reaction (diffusion) time, we consider the system to be in a diffusion (reaction) controlled regime.

At the beginning of a typical simulation, 100 trial runs are performed to calculate the average reaction half-life. This average value is compared to the corresponding relevant characteristic diffusion time, and the larger of the two serves as the "characteristic time" for the simulation. Without inhibition, each simulation is run for 10 characteristic times, to ensure a quasi-steady state has been achieved. When strong inhibition is present, the simulations are lengthened to 20 characteristic times in order to accommodate the significantly slower dynamics, as will be explained later.

In this work, as done previously,[51] we define a symmetry breaking transition to occur when the sample skewness of the probability distribution of the absolute value of enantiomeric excess, $Q(|ee|)$, becomes negative. The sample skewness is a convenient parameter to quantify symmetry breaking because it relates to the unimodal/bimodal character of the probability distribution function of the absolute value of the enantiomeric excess. The sample skewness is written as

$$g = \frac{\sqrt{n_s(n_s - 1)}}{n_s - 2} \frac{m_3}{{m_2}^{3/2}} \tag{2}$$

where g = sample skewness of $Q(|ee|)$, n_s = number of independent simulations, m_2 = second central moment of $Q(|ee|)$, m_3 = third central moment of $Q(|ee|)$, $ee = (N_R - N_S)/(N_R + N_S)$, and N_i is the number of chiral molecules of enantiomer i. Note that the enantiomeric excess is defined here as an overall enantiomeric excess, which accounts for all chiral product molecules, including those that have formed a heterochiral dimer complex, D.

For a given set of simulation parameters, n_s = 10 000 independent simulations are performed to ensure adequate sampling, and the $Q(|ee|)$ curve is constructed from the final enantiomeric excess of each of these runs. The sample skewness is then calculated from this probability distribution, and if its value is less than zero, the system is said to have achieved a (quasi-steady) symmetry-broken state. Further details are provided in the Appendix.

III. PARAMETER SPACE

Figure 2 is a schematic depiction of the energy barriers for the reaction system involving the production of C. As one can see, only three of the four energy barriers are independently variable.

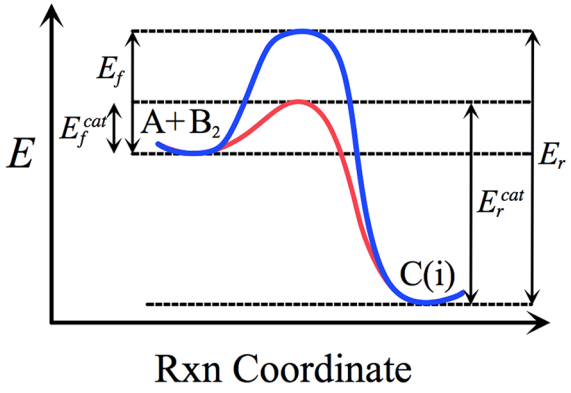

Figure 2. Schematic of energy barriers to reaction for the formation and decomposition of chiral product (C). The blue line represents the noncatalytic pathway and the red line represents the autocatalytic pathway (i.e., in the forward direction: $A + B_2 + C(i) \rightarrow 2C(i)$, $i = \{R, S\}$).

To represent the parameter space explored in this study, we define three activation energy ratios: $r = E_f/E_r$, $p = E_f^{cat}/E_r^{cat}$, and $\alpha = E_f^{cat}/E_f$. Figure 3 shows the relationship between r and p along loci of constant α, which is described mathematically by eq 3. We restrict ourselves to $E_f \leq E_r$ or, equivalently, $r \in [0,1]$, $p \in [0,1]$, $p \leq r$.

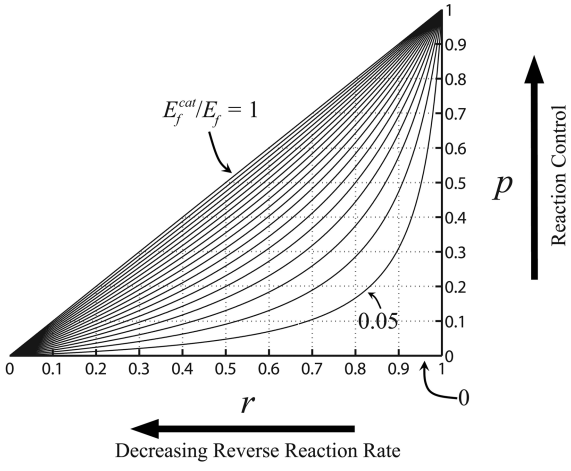

Figure 3. Parameter space represented on a triangular chart. Curves of constant $\alpha = E_f^{cat}/E_f$ are shown spanning the range [0, 1] in increments of 0.05.

$$p = \frac{\alpha r}{(\alpha - 1)r + 1} \tag{3}$$

dx.doi.org/10.1021/jp3093644 | J. Phys. Chem. B 2013, 117, 602−614

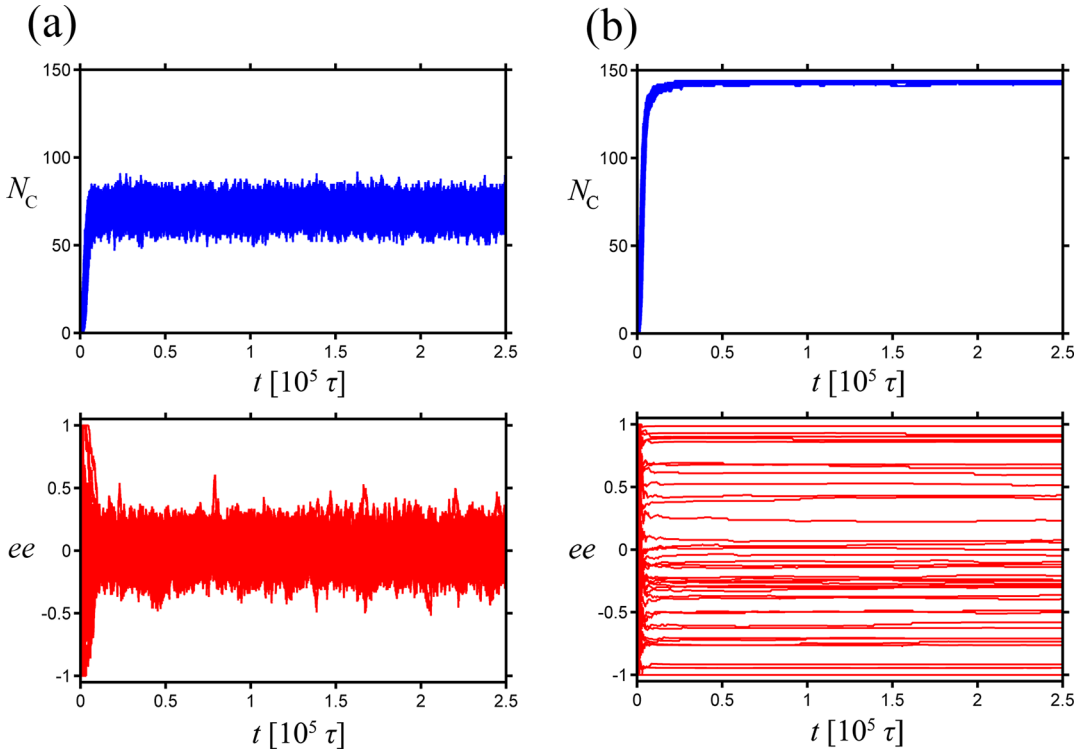

Figure 4. Time trajectories of the number of chiral product molecules (N_C) and the corresponding enantiomeric excess (ee) for two sets of 40 independent simulation runs having different reverse reaction rates. (a) $r = E_f/E_r = 1$ (equi-energetic reactants and products). (b) $r = E_f/E_r = 0.5$. Both sets of simulations were performed without inhibition ($\varepsilon/E_f = 0$) and with all other independent parameters equal: $\beta E_f = 10$, $E_f^{cat}/E_f = 0$, $\varphi = 1/3$, and $n = 36$. These simulations were run for ~10 characteristic diffusion times. Since there is no inhibition, $N_C = N_R + N_S$.

Also indicated on the diagram in Figure 3 are the directions of decreasing r ($=E_f/E_r$), corresponding to a decreasing reverse reaction rate ($E_r \gg E_f$), and of increasing p ($=E_f^{cat}/E_r^{cat}$). In the latter case, as one traverses higher and higher values of α ($=E_f^{cat}/E_f$) by increasing p at fixed r, the difference between the energy barrier heights for the autocatalytic and noncatalytic reactions lessens, and the overall reaction rate slows, indicated by the "reaction control" arrow. As α approaches unity, the energy barriers for the autocatalytic and noncatalytic reactions become the same and the autocatalytic mechanism ceases to be "catalytic" (we neglect molecularity considerations for the moment, though they also play a role in the rates of reaction). The remaining variables not shown on the triangular chart are temperature, coverage fraction, and system size.

IV. RESULTS AND DISCUSSION

It has been firmly stated[55] that linear autocatalysis alone cannot cause chiral symmetry breaking. However, Hatch et al.[51] did indeed identify conditions leading to substantial enantiomeric excess with linear autocatalysis in the absence of inhibition. These authors observed that the conditions required for symmetry breaking without inhibition in their elementary lattice model involve significantly lower temperatures than in the presence of inhibition, such that a "single mother mechanism" might be effective in propagating the handedness of the first chiral molecule formed. This mechanism is based on the simple fact that, whenever there is a difference in activation energies between two reactions (i.e., $E_f^{cat} < E_f$), the ratio of their rate constants ($k_f^{cat}/k_f \sim \exp[\beta\,(E_f - E_f^{cat})]$) becomes arbitrarily large as the temperature decreases. It is easy to visualize the implications of this fact through a simple thought experiment: consider the 2-D lattice system initially populated with only reactants. As the reactant molecules diffuse, the first reaction to occur must necessarily be noncatalytic, and therefore the handedness of the first C molecule (R or S) is completely random. If the temperature of the lattice system is sufficiently low, the rate of the autocatalytic reaction will be much faster than that of the noncatalytic reaction, such that the first "mother" C molecule will spread via diffusion and propagate its own handedness through autocatalysis before the next random nonautocatalytic reaction takes place. In the extreme case, the first C molecule is able to propagate its own type so quickly that all of the reactant is exhausted before the next nonautocatalytic event, necessarily resulting in an enantiopure system. On the other hand, as $\beta \to 0$ the difference in activation energies is irrelevant and the random nonautocatalytic reactions should statistically drive the system toward a racemic mixture of C molecules.

By adding reaction reversibility in a system without mutual inhibition, we observe that, for appreciable reverse reaction rates, any initially formed enantiomeric excess quickly degrades to racemic on the same time scale as the formation of the chiral molecules themselves (Figure 4). However, as the reverse reaction rate is lowered, a separation of time scales occurs, wherein the initially formed enantiomeric excess achieves a quasi-steady state, with the decay to equilibrium lasting extremely long times. For progressively slower reverse reaction rates, one can produce and maintain chiral asymmetry for arbitrarily long times. While some of the simulations in Figure 4b result in little enantiomeric excess, others form an enantiopure "final" mixture at quasi-steady state. As illustrated by Hatch et al.,[51] decreasing the temperature would increase the probability of observing an enantiopure quasi-steady state.

dx.doi.org/10.1021/jp3093644 | J. Phys. Chem. B 2013, 117, 602−614

The trajectories depicted in Figure 4b demonstrate that slow reverse reaction rates cause a separation of time scales between the formation of C molecules and achieving racemic equilibrium. Allowing such a simulation to achieve racemic equilibrium would be computationally prohibitive due to the slow reverse reaction rates. Therefore, we instead opt to give the system a "thermal boost" in order to see whether it will inexorably tend to racemic equilibrium. Figure 5 depicts 40

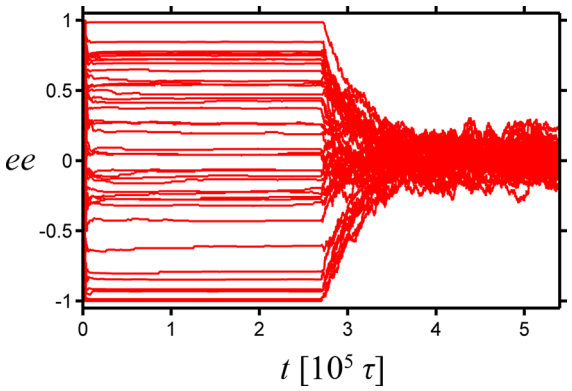

Figure 5. Time trajectories of the enantiomeric excess (ee) for 40 independent simulation runs, with the addition of a "thermal boost" midway through each simulation. βE_f(initial) = 10; βE_f(final) = 5. All simulations were performed with r = 0.5, ε/E_f = 0, E_f^{cat}/E_f = 0, φ = 1/3, and n = 36.

independent simulations run under conditions identical to those depicted in Figure 4b; however, after the simulations have run for 10 diffusion characteristic times, the temperature is increased by a factor of 2 and the simulation continues to run for another 10 characteristic diffusion times. The trajectories clearly indicate that the imposition of a "thermal boost" rapidly carries the system to the racemic equilibrium state. Moreover, if the temperature is then restored to its original value (not shown) the system remains racemic, thereby implying that the slowly evolving system in Figure 4b will eventually become racemic.

While our model illustrates a separation of time scales and substantial symmetry breaking for systems without mutual inhibition, it is apparent that inhibition between competing enantiomers should greatly enhance the extent of symmetry breaking, and also expand the range of parameter space over which symmetry breaking may occur. For example, Hatch et al. demonstrated that strong mutual inhibition (ε/E_f = 10) allowed their model to break symmetry at significantly higher temperatures and also exhibit system-size independence in the reaction controlled regime.[51] Of course, those results were observed in a system with no reverse reactions.

Figure 6 illustrates how strong mutual inhibition affects systems with appreciable reverse reaction rates. Both sets of simulations in this Figure 6 were performed with r = 0.9, and the resulting effect of high reverse reaction rates can be seen by the large fluctuations in the enantiomeric excess. One should note that the two graphs are plotted on different time scales, with Figure 6b spanning one additional order of magnitude. The simulations without inhibition rapidly approach equilibrium, with all 40 runs achieving a racemic mixture by approximately $10^5\tau$. However, the simulations with strong inhibition show markedly different behavior. In this case, all 40 runs show strong early-time symmetry breaking, followed by a comparatively slower approach to racemic equilibrium. At this set of conditions the inclusion of strong inhibition lengthens the racemization time by over an order of magnitude.

This drastic slowing of the system's dynamics, and resulting lengthening of the racemization time, is due to an "irreversible" sink mechanism caused by the strong association between heterochiral pairs of enantiomers. As soon as a molecule of the minor enantiomer is formed, it rapidly associates with an uninhibited (i.e., free) molecule of the major enantiomer, forming a heterochiral dimer. The relatively fast rate of dimerization effectively creates a prolonged nearly homochiral regime for the uninhibited (monomeric) chiral molecules, which we refer to as the "monomer purification" mechanism. This behavior is depicted in Figure 7, wherein the adjusted enantiomeric excess (ee_{adj}) only accounts for the enantiomeric excess within the population of uninhibited (monomeric) chiral molecules. The adjusted enantiomeric excess is calculated as $ee_{adj} = (N_{R,un} - N_{S,un})/(N_{R,un} + N_{S,un})$, where the subscript "un" denotes "uninhibited".

Referring to Figure 7, it can be seen that the number of achiral reactant molecules and monomeric chiral product

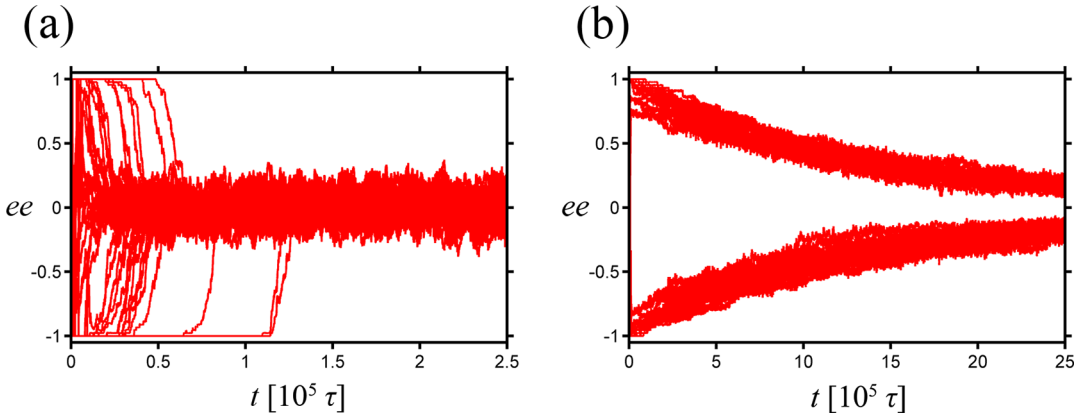

Figure 6. Time trajectories of the enantiomeric excess (ee) for two sets of 40 independent simulation runs having different dimer binding energies. (a) ε/E_f = 0 (no inhibition), run for ~10 characteristic diffusion times. (b) ε/E_f = 10 (strong inhibition), run for ~60 characteristic diffusion times to illustrate long-time behavior. Both sets of simulations were performed with all other parameters equal: βE_f = 12, $r = E_f/E_r$ = 0.9, E_f^{cat}/E_f = 0, φ = 1/3, and n = 36. When inhibition is present, the reported ee is the "overall" enantiomeric excess, which includes the chiral product molecules arrested in heterochiral dimers.

dx.doi.org/10.1021/jp3093644 | J. Phys. Chem. B 2013, 117, 602−614

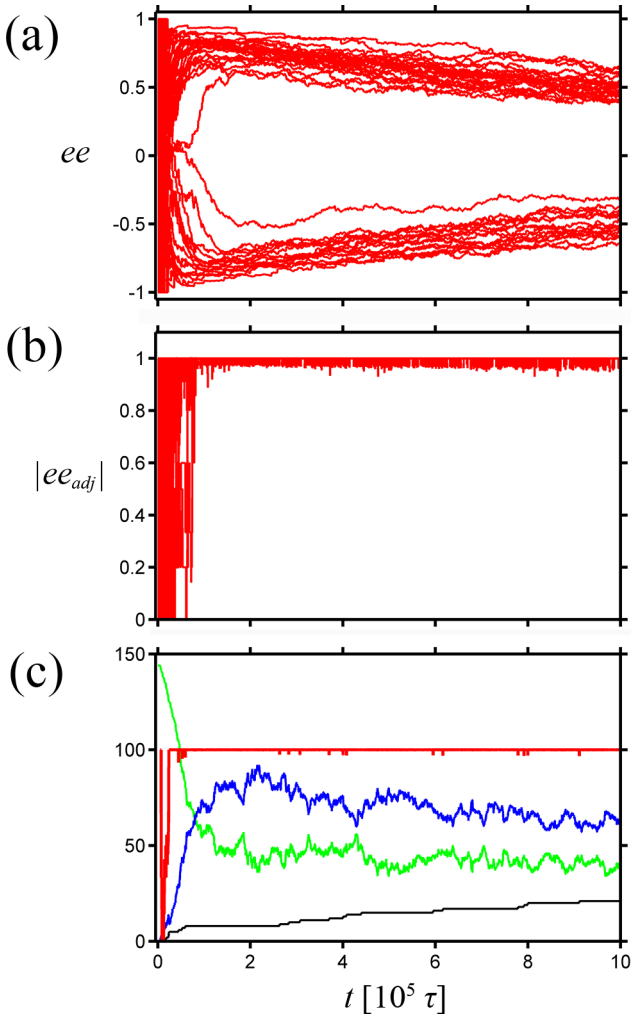

Figure 7. Illustration of the "monomer purification" mechanism. (a) Time trajectories of the overall enantiomeric excess (ee) for 40 independent simulations. (b) Corresponding time trajectories of the absolute value of the adjusted (monomer-only) enantiomeric excess ($|ee_{adj}|$) for the 40 independent simulations. (c) A typical trajectory for a single run, including the numbers of all molecules. Red line = $|ee_{adj}|\cdot 100$, green line = $N_A = N_B$, blue line = N_C, and black line = N_D. All simulations performed with $\beta E_f = 12$, $r = E_f/E_r = 0.88$, $\varepsilon/E_f = 10$, $E_f^{cat}/E_f = 0.35$, $\varphi = 1/3$, and $n = 36$. Note, N_B denotes the number of B_2 molecules, and furthermore, $N_A = N_B$ is satisfied at all times since all simulations begin with an equimolar mixture of reactants.

molecules decreases steadily over long times while the number of dimers increases monotonically. Despite the fact that the reverse reaction rate is appreciable ($r = 0.88$), near homochirality of the chiral monomers is still preserved. Notice that when the system achieves quasi-steady state any small departures from enantiopurity in the chiral monomer population quickly disappear, coinciding with an instantaneous increase in the number of heterochiral dimers. In essence the strong dimerization "purifies" the population of uninhibited chiral molecules by quickly removing any newly formed molecules of the minor enantiomer. As such, only the major enantiomer is available to partake in autocatalysis, thereby forming a quasi-steady nearly homochiral state. As a result, the overall enantiomeric excess (ee) decays steadily while the absolute value of the adjusted enantiomeric excess ($|ee_{adj}|$) remains ~1. The enantiopurity created by this mechanism persists until the number of chiral monomers becomes so small that each newly formed C molecule takes a very long time to find a C molecule of the opposite handedness and dimerize.

Figure 8 illustrates the "monomer purification" mechanism with varying rates of autocatalysis, such that the reaction half-life of A in Figure 8b is over an order of magnitude longer than that in Figure 8a. The slower autocatalysis in Figure 8b allows the formation of more monomers of the minor enantiomer at early times. As a result, it takes slightly longer until near homochirality is achieved. Despite the differences in the rate of autocatalysis, each system's quasi-steady behaviors are qualitatively similar to each other, indicating that this mechanism is robust over a range of autocatalytic reaction rates.

The rates of reverse reaction depicted in Figures 7 and 8 are quite significant, as evidenced by the large fluctuations in particle number. As the rates of reverse reaction are lowered by decreasing r, the persistence time of the nearly homochiral monomer state increases drastically. In the limit where there are no reverse reactions ($r = 0$) all monomers of the minor enantiomer will eventually dimerize, leaving an enantiopure pool of monomers for arbitrarily long times. If these chiral monomers were then capable of polymerizing, or forming homochiral aggregates, this prolonged homochiral regime would be favorable for the creation of more complex homochiral biotic building blocks.

The above mechanism can be qualitatively likened to the thermodynamic mechanism for liquid phase enantioenrichment in ternary (liquid−solid−solid) phase equilibria.[2,4] In these systems, even a slight chiral imbalance is amplified in the liquid phase due to the formation of a sparingly soluble racemic crystal. In simple terms, the minor enantiomer becomes "arrested" within the racemic crystal, enriching the liquid phase enantiomeric excess. In the present model, the heterodimer is analogous to the racemic crystal. While the thermodynamic phase partitioning in real systems requires the input of an initial chiral imbalance, the present model is capable of spontaneously generating the required imbalance with no biasing, just as the Soai reaction is able to spontaneously break symmetry without intentional bias.[39] The key difference is that in our model the near enantiopurity of uninhibited C molecules is a "far from equilibrium" kinetic phenomenon, not a consequence of thermodynamic equilibrium.

To see how temperature affects the extent of symmetry breaking, we return to the triangular p vs r diagram. The present model does not contradict the statement that, for a closed system satisfying microscopic reversibility, the racemic equilibrium state is inevitable at long times. However, the model allows investigation of how long it takes to achieve a nearly racemic state. We define symmetry breaking by the condition $Q < 0$ [see eq 2] and adopt the criterion that a state of broken symmetry lasting more than 10 (20) characteristic times is considered significant in the absence (presence) of inhibition. The main purpose of defining characteristic times is pragmatism, and maintaining a symmetry-broken state for 10−20 characteristic times is significant from an order of magnitude perspective in that it represents maintaining symmetry breaking for at least 1 order of magnitude longer than the characteristic time of the system.

When the reverse reaction rate is too high (increasing r), the system cannot maintain a symmetry-broken state. As r is decreased along a curve of constant E_f^{cat}/E_f [α in eq 3], there may exist a symmetry breaking transition point at which the system can maintain symmetry breaking for 10 (20) character-

dx.doi.org/10.1021/jp3093644 | J. Phys. Chem. B 2013, 117, 602−614

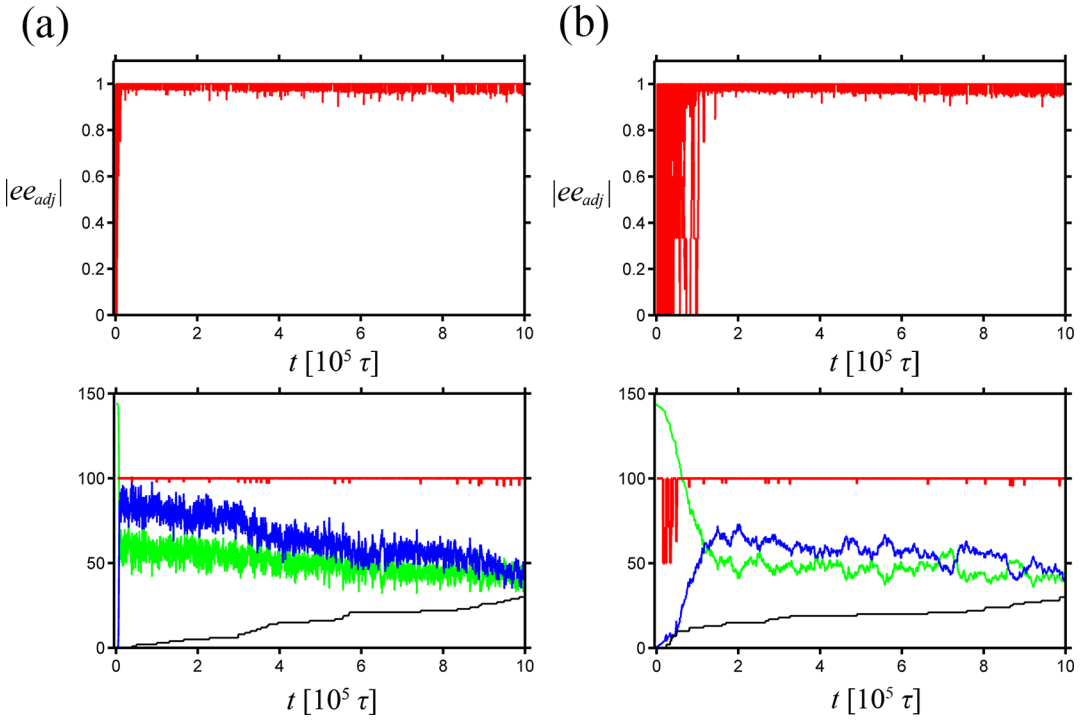

Figure 8. Illustrations of the monomer purification mechanism with differing rates of autocatalysis. (top) Time trajectories of the absolute value of the adjusted enantiomeric excess ($|ee_{adj}|$) for 40 independent simulations. (bottom) A typical trajectory for a single run from the above 40 simulations. Red line = $|ee_{adj}|\cdot 100$, green line = $N_A = N_B$, blue line = N_C, and black line = N_D. (a) $E_f^{cat}/E_f = 0$, and reaction half-life for $A = 6700\tau$. (b) $E_f^{cat}/E_f = 0.35$, and reaction half-life for $A = 75000\tau$. For both sets of simulations $\beta E_f = 12$, $r = E_f/E_r = 0.9$, $\varepsilon/E_f = 10$, $\varphi = 1/3$, and $n = 36$. The characteristic diffusion time for C at these conditions is 39000τ.

istic times in the absence (presence) of inhibition. As one continues to decrease r at constant E_f^{cat}/E_f, decreasing the reverse reaction rate further, the persistence time of symmetry breaking continues to increase precipitously, reaching infinity in the limit $r = p = 0$. Figure 9 illustrates the regions of parameter space over which symmetry breaking can be created and maintained from a minimum of 10 or 20 characteristic times at the symmetry breaking transition line to a maximum of infinite time at $r = p = 0$.

Figure 9 clearly shows that upon lowering the temperature (increasing βE_f) the reverse reaction takes progressively longer to bring the system to equilibrium, thereby expanding the region over which symmetry breaking persists. Moreover, inhibition expands the symmetry-broken region over the case of no inhibition. When the system is at high enough temperature ($\beta E_f = 8$), simulations without mutual inhibition cannot produce symmetry breaking in the limit of a completely irreversible reaction, which is in agreement with the findings of Hatch et al.[51]

As one increases p at constant r, slowing the effective rate of autocatalysis, there comes a point at which autocatalysis becomes so slow that it is irrelevant. When autocatalysis is no longer a viable means of providing competition between enantiomers, the system can no longer break symmetry. Hence, the shaded regions in Figure 9 are limited by some upper value of α, above which symmetry breaking does not persist, even in the limit of a completely irreversible reaction ($r = p = 0$).

System size effects were also explored for three cases: 18 × 18, 36 × 36, and 60 × 60 lattices. All system sizes showed the same qualitative behavior. For larger system sizes, reverse reaction rates must be lower in order to preserve symmetry breaking for the requisite amount of time. However, when

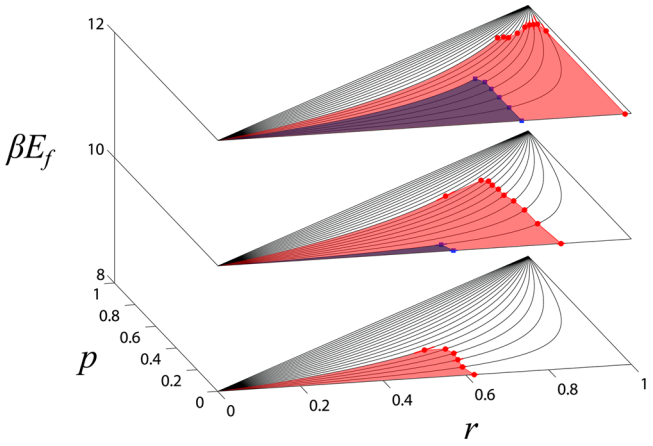

Figure 9. Regions of symmetry breaking as a function of temperature ($\beta = 1/k_BT$). The blue squares represent the symmetry breaking transition points for simulations with no inhibition ($\varepsilon/E_f = 0$), while the red circles are the symmetry breaking transition points for strong inhibition ($\varepsilon/E_f = 10$). These points are defined such that, when r is decreased along a curve of constant E_f^{cat}/E_f [α in eq 3], persistent symmetry breaking lasting more than 10 (20) characteristic times in the absence (presence) of inhibition is first encountered. The overlapping regions shaded in blue ($\varepsilon/E_f = 0$) and red ($\varepsilon/E_f = 10$) represent the parameter space over which symmetry breaking is expected to form and persist for more than 10 or 20 characteristic times, respectively. All simulations were performed with $\varphi = 1/3$ and $n = 36$.

inhibition is present, the symmetry breaking transition lines start to converge as E_f^{cat}/E_f is increased to >0.30, indicating the transition to a reaction controlled regime.

dx.doi.org/10.1021/jp3093644 | J. Phys. Chem. B 2013, 117, 602−614

V. IMPLICATIONS FOR THE ORIGIN OF BIOLOGICAL HOMOCHIRALITY

In this section, we explore some possible implications of the phenomenology illustrated in Figures 4−8 for the origin of biological homochirality. In order to facilitate this discussion, reaction rate constants are calculated based on transition state theory (TST).[56] For a liquid-phase reaction, one may derive the TST equation for a general reaction rate constant, k:

$$k = \frac{k_B T}{h}\rho^{\sum_i \upsilon_i}\prod_i \gamma_i^{-\upsilon_i}\prod_i (x_i^\circ)^{\upsilon_i}\exp[\Delta S^*/k_B]\exp[-\Delta H^*/k_B T] \quad (4)$$

where h = Planck's constant, ρ = total molar density of reaction solution, γ_i = activity coefficient of reaction species i, utilizing infinite dilution normalization, υ_i = stoichiometric coefficient of reaction species i, x_i° = reference state mole fraction of reaction species i, ΔS^* = entropy of activation, and ΔH^* = enthalpy of activation. Equation 4 is amenable to several simplifying assumptions. First, for order of magnitude calculations one may assume that the enthalpy of activation is equal to the reaction activation energy ($\Delta H^* = E_a$). Since the activity coefficients are normalized with the infinite dilution convention, one may assume that if the reactants are sufficiently dilute $\gamma_i \approx 1$ for all species i. Furthermore, since one may arbitrarily choose the reference state mole fractions, x_i°, we define them such that their product in eq 4 is $\sim O(1)$. With these assumptions, the above equation reduces to

$$k = \frac{k_B T}{h}\rho^{\sum_i \upsilon_i}\exp[\Delta S^*/k_B]\exp[-E_a/k_B T] \quad (5)$$

If one assumes that the reaction occurs in a dilute aqueous solution, as we do in subsequent calculations, then ρ is approximately equal to the molar density of water at the system temperature. Values of ΔS^* have been tabulated for certain reactions, and theoretical prediction techniques have also been developed through statistical mechanics.[56,57] After choosing an appropriate value of ΔS^*, k is readily calculated for any value of E_a at a given temperature.

Consider for illustrative purposes the case of strong mutual inhibition between enantiomers, which facilitates the monomer purification mechanism. When the reverse reaction rates are extremely slow ($r \to 0$), the reaction goes to completion, and the strong inhibition causes nearly all of the minor enantiomers to form heterodimers, leaving a homochiral pool of monomeric C molecules. Under these conditions, racemization will take an exceedingly long time. However, this is trivially expected whenever the reverse reaction rates are low in such a system. Therefore, it is much more informative to observe the case of monomer purification coupled with appreciable reverse reaction rates.

Consider the regime in which there is strong mutual inhibition and also appreciable reverse reaction rates, such that the C molecules continually decompose back to A and B_2. This scenario is depicted in both Figures 7 and 8. It can be seen that a long evolution toward chiral symmetry characterizes the system's behavior. We wish to quantify the duration of such a long transient during which the system evolves toward equilibrium following the autocatalytically propagated early symmetry breaking event. As explained in section IV, during the system's slow evolution toward chiral symmetry, the adjusted enantiomeric excess of free chiral molecules rarely deviates from unity, indicating a homochiral population of unassociated (monomeric) C molecules. Intermittently, a C molecule of the "wrong" (minority) chirality is formed, and the adjusted enantiomeric excess briefly deviates from unity. Since the number of heterochiral dimers does not decrease during these excursions from homochirality, the C molecule of the "wrong" chirality was necessarily formed via the nonautocatalytic reaction A + $B_2 \to$ C. However, this C molecule is surrounded by C molecules of opposite handedness, and therefore it quickly becomes arrested in a heterochiral dimer, thereby restoring homochirality in the monomer population and inching the system toward racemic equilibrium. Therefore, in this regime it is the nonautocatalytic formation of C molecules of the minor handedness which limits the rate of racemization. We focus on this reaction in the ensuing calculations.

It was confirmed by the method of initial rates[44] that this reaction is second order, as implied by its molecularity (see the Appendix). The characteristic time for a second order reaction is given by

$$t_R = \frac{1}{k[A]_0} \quad (6)$$

where $[A]_0$ is the initial concentration of reactant A and t_R is the reaction half-life, that is, the time it takes for [A] to decrease to [A]/2. For the forward noncatalytic reaction $k = k_f$, and since this reaction governs the time scale of racemization, t_{rac}, we write

$$t_{rac} = \frac{1}{k_f[A]_0^{QS}} \quad (7)$$

where $[A]_0^{QS}$ denotes the concentration of A at the onset of the "quasi-steady state".

Using typical values for ΔS^* and E_f for bimolecular reactions,[56−58] $\Delta S^* = -125$J/mol·K and $E_f = 75$ kJ/mol; along with $T = 300$ K and $[A]_0^{QS} = 10^{-5}$ M (a reasonable concentration for a biological metabolite), eqs 5 and 7 together yield $t_{rac} \sim 10^6$ years. This mechanism therefore clearly illustrates a plausible route by which a nearly enantiopure population of chiral monomers can be maintained for long times, even with high reverse reaction rates. This value of the activation energy combined with $T \sim 300$ K yields $\beta E_f = 30$, a parameter range that we did not explore because of the extremely low acceptance probabilities associated with such Boltzmann factors [$O(10^{-13})$]. Such low acceptance probabilities would have made the problem computationally intractable with our explicit kinetic Monte Carlo.

In order to compare the diffusion time in a macroscopic system to the reaction time estimated above, we consider a macroscopic aqueous pool with a characteristic length of ~1 m. Assuming that the chiral molecule of interest, equivalent to our C molecule, has a diffusivity comparable to that of an amino acid (i.e., serine), we take the diffusivity to be $\sim 10^{-5}$ cm^2/s. The characteristic diffusion time is defined in a fashion similar to that of eq 1:

$$t_D = \frac{L^2}{6D} \quad (8)$$

where L = characteristic length scale and D = diffusivity of the component of interest. The resulting diffusion time is ~5 years. Of course, this value is an upper limit and also a drastic overestimate, in that it assumes that the pool of interest remains perfectly static, with diffusion acting as the only transport

dx.doi.org/10.1021/jp3093644 | J. Phys. Chem. B 2013, 117, 602−614

mechanism. Environmental factors such as wind and thermal convection would reduce this number to a much smaller value, likely orders of magnitude smaller. Comparing t_D to a racemization time which could be in excess of 1 million years, it is clear that, for reasonable values of the relevant physical parameters, the time scale of racemization is many orders of magnitude larger than the time scale for diffusion, and the macroscopic pool would then behave as a single domain.

In closing this section, we make an observation on the relationship between the coverage fraction employed in this study ($\varphi = 1/3$) and the reactant concentration in an actual solution. Consider the 36 × 36 system at 1/3 coverage, which contains initially 144 A molecules, 144 B_2 molecules, and no C molecules. Assuming that the chiral molecule of interest is an amino acid such as serine, comparison to a C molecule indicates that the lattice constant, l, is approximately 3 Å. If we consider the two-dimensional system to represent a slice of thickness l in a three-dimensional solution, then the 36 × 36 × 1 system has a volume of 35 × 10^3 Å^3. The effective initial concentration of A molecules is then ∼7 M, which is between 5 and 6 orders of magnitude larger than the value assumed for the concentration in the racemization time calculation. Thus our simulations are performed under highly concentrated conditions. This is only due to numerical considerations since, if one were to run simulations at very high dilutions, the simulation times would become enormous, making the problem computationally infeasible.

VI. CONCLUSION

The elementary model studied herein is capable of breaking chiral symmetry with explicitly chiral entities, molecular degrees of freedom, and no initial geometric bias for symmetry breaking. With the inclusion of reverse reaction rates, the model satisfies microscopic reversibility and evolves inexorably toward the racemic equilibrium state over long enough times. Numerical investigation of the model's behavior has enabled us to identify conditions under which the system's evolution toward racemic equilibrium following an initial symmetry breaking event becomes extremely slow, and chiral imbalance can be maintained over very long times. Strong mutual inhibition between enantiomers, as well as low temperatures, leads to this type of behavior. Conversely, when the activation rates of the forward autocatalytic and noncatalytic reactions become sufficiently similar, symmetry breaking cannot occur. Strong mutual inhibition leads to the monomer purification mechanism, which allows long-time persistence of a nearly homochiral state even in the presence of significant reverse reaction rates. Hence, strong mutual inhibition not only enhances the initial symmetry breaking event, but can also greatly lengthen the persistence time of symmetry breaking in such systems. Order of magnitude estimates based on realistic reaction rate constants indicate that a nearly enantiopure population of chiral monomers can be preserved for geologically relevant times in a system closed to mass flow, even with significant reverse reaction rates. This suggests a plausible scenario for the spontaneous emergence of homochirality in a system of macroscopic dimensions. Our study thus adds to the rich variety of plausible scenarios for the emergence and maintenance of homochirality in a presumably racemic prebiotic world.

For all cases examined with nonvanishing reverse reaction rates, the final equilibrium state involves a distribution of enantiomeric excess which fluctuates narrowly around zero, i.e., a symmetric unimodal distribution. However, that is not the only conceivable scenario. A broader family of models could include additional intermolecular interactions of intermediate range which are attractive for homochiral pairs of chiral product molecules and repulsive for heterochiral pairs. If these additional interactions were sufficiently strong compared to k_BT, and the concentration of product molecules sufficiently high, liquid immiscibility could result. The final equilibrium state for an ensemble of such systems could then involve a bimodal distribution of enantiomeric excess. At any given moment of observation one would encounter a dominantly chiral overall state. Eventually a sufficiently powerful and properly directed thermal fluctuation could switch the system to the other half of the bimodal distribution, but the mean persistence time between such switches would depend on the free energy of a transition state which can be very large compared to k_BT. An informative analogy may be a finite-size Ising ferromagnet in contact with a heat bath below the Ising critical temperature; its thermal equilibrium state would involve equally probable "up" and "down" magnetizations with long persistence times.

Our study suggests several directions for future inquiry. We have so far considered thermodynamic[4] and kinetic[51] models for the amplification of chiral imbalance. It would be interesting to combine both models, bridging far-from-equilibrium kinetics with equilibrium thermodynamics. Important effects, such as convection, have not been considered so far by us. Extending our studies and calculations to three dimensions and developing models that can shed light on chiral symmetry breaking in crystallizing systems subject to the input of mechanical energy[12,14] also appear to be fruitful directions for future work.

APPENDIX

Species Description

Reactant A. Species A can diffuse in any of four directions on the 2-D lattice and can react with species B_2 via noncatalytic and autocatalytic routes to form product C.

Reactant B_2. Species B_2 can diffuse in any of four directions, can perform a 90° rotation (whereby one of the subunits remains stationary), and can react with species A via noncatalytic and autocatalytic routes to form product C.

Product C (Chiral Monomer). Species C exists in either of two chiral forms (herein denoted "R" and "S"). This species can diffuse in any of four directions, can perform a 90° rotation (whereby the vertex subunit remains stationary), can decompose to A and B_2 via noncatalytic and autocatalytic routes, and can associate with a C molecule of the opposite chirality.

Associated Complex D (Chiral Heterodimer). Species D can diffuse in any of four directions and can dissociate to C(R) and C(S).

Characteristic Times

The diffusivities of species A, B_2, and C are calculated by using the Einstein expression:

$$D_i = \frac{\langle (\delta r)^2 \rangle}{2dt} \tag{A.1}$$

where D_i = diffusivity of species i in units of $[l^2/\tau]$ (τ is the inherent unit of time associated with the kinetic MC algorithm), $\langle (\delta r)^2 \rangle$ = mean square displacement of species i in the time interval of length t, d = dimensionality of the system

dx.doi.org/10.1021/jp3093644 | J. Phys. Chem. B 2013, 117, 602−614

(2 for this model), and t = time. Since during a simulation reactions cause the mixture composition to change with time, we investigated the effect of composition on diffusion coefficients. To measure the effective diffusion of particles during a reactive simulation while maintaining a constant mixture composition, we use "mock reactions" while measuring D_i. When mock reactions are used, any (randomly) selected particle is randomly chosen to either diffuse or react, as it would be in a typical simulation; however, if the particle is selected to react, nothing occurs and the time is advanced by $(1/N)\tau$. In this way, the mixture composition remains constant while recording diffusivities. Without using mock reactions, every time a particle is selected it automatically attempts a diffusive move, causing the particles to diffuse approximately twice as fast as in a simulation with reactions. As shown in Figure 10,

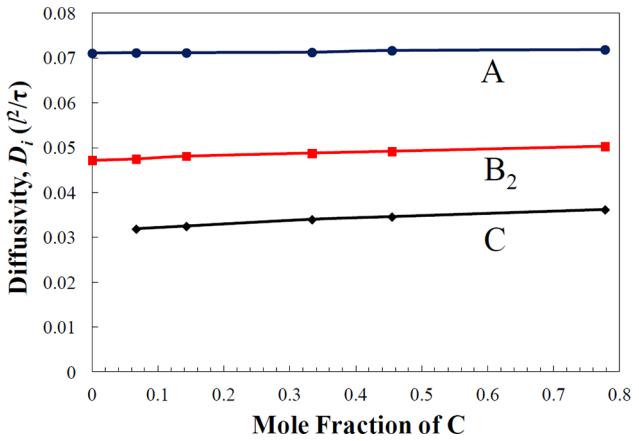

Figure 10. Diffusivity as a function of composition (φ = 1/3) for a mixture with equimolar amounts of A and B_2 and "mock reaction" employed.

the diffusivities are not strong functions of mixture composition for a coverage fraction of 1/3. Therefore, for the purpose of estimating a characteristic diffusion time, the composition dependence of D_i is neglected.

The characteristic diffusion time of species i, defined here as the approximate time it takes for a molecule of said species to diffuse the length of the system, is calculated by a modified version of eq A.1:

$$t_{d,i} = \frac{(nl)^2}{D_i} \tag{A.2}$$

where $n = n_x = n_y$ (system size) and l = width of a lattice site. For estimation purposes, we use the diffusivities for an equimolar ternary mixture. For a 36 × 36 lattice, the resulting characteristic diffusion times are then $t_{d,A} = 18000\tau$, $t_{d,B_2} = 27000\tau$, and $t_{d,C} = 39000\tau$. In a simulation without inhibition, species B_2 is taken to define the characteristic diffusion time. In the presence of inhibition, time scales are significantly longer and the diffusion of C plays a role in dimer formation; therefore, the characteristic diffusion time of C is used instead.

The reaction half-life is utilized as a characteristic reaction time scale. It is approximated for each set of reaction conditions by running 100 independent trials, during which the number of A molecules is tracked. When the moving-average number of A molecules drops below half its initial value, the half-life is recorded (the moving average is computed by using 99 preceding points and the current point, each separated by 1τ). The results of the 100 independent trials are averaged to obtain an average reaction half-life. The reaction half-life may vary greatly under different conditions. Indeed, under some conditions reaction equilibrium may preclude the consumption of more than half the initial reactants, or under certain circumstances the reaction takes so long to achieve equilibrium that the time evolution of the number of reactant molecules becomes prohibitively slow. If 10 out of 100 trial runs exhibit a failure to achieve half the initial value of A, the simulation reverts to using the 3/4-life, though this is quite a rare occurrence in the parameter ranges explored in this study. One should note that this definition of reaction time is not intended to be a precise quantification, but rather an indicator for the relative rates of reaction and diffusion.

Simulation Trials

The reaction half-life is compared to the characteristic diffusion time of choice (either B_2 or C, depending on the presence or absence of inhibition), and whichever time scale is larger is chosen as the characteristic time scale for that particular set of reaction conditions. The trial runs are then carried out for 10 or 20 characteristic times, depending on the presence or absence of inhibition, respectively. This is done to ensure that the particle numbers have achieved a quasi-steady state and that the system has had adequate diffusion time by the end of the simulation.

At the conclusion of a trial run (after the requisite time has elapsed), the average particle numbers and average overall enantiomer fraction, f, are calculated on the basis of the last 1/3 of the data for that particular run (note $f = N_R/(N_R + N_S)$, which does not distinguish between inhibited and uninhibited C molecules). The first 2/3 of the trajectory is omitted in an effort to exclude any early-time transient behavior in the particle numbers. This procedure is repeated 10 000 times per each set of reaction conditions, and a probability distribution function, $Q(f)$, is recorded by binning the final values of f for all runs and normalizing by the total number of runs.

As mentioned in section II, the sample skewness is a convenient quantity in terms of defining the symmetry breaking transition since it is well-defined mathematically and relates to the unimodal/bimodal character of the probability distribution function of the absolute value of the overall enantiomeric excess, $Q(|ee|)$, which is linearly related to the $Q(f)$ via $|ee| = |2f - 1|$.

Method of Initial Rates

The method of initial rates[44] was used in order to determine reaction order for all the reactions in our model. For instance, in the noncatalytic reaction A + B_2 → C(i), where i = R or S, the molecularity implies that the reaction is second order. In order to rigorously demonstrate the overall reaction order, we first postulate the general rate law:

$$r = -\frac{dC_A}{dt} = k_f C_A^{\eta} C_{B_2}^{\xi} \tag{A.3}$$

where r = reaction rate [molecules/$n^2\tau$], k_f = reaction rate constant [(molecules/n^2)$^{1-(\eta+\xi)}/\tau$], C_A = concentration of A molecules [molecules/n^2], C_{B_2} = concentration of B_2 molecules [molecules/n^2], η = reaction order with respect to species A, and ξ = reaction order with respect to species B_2.

Equation A.3 may be rewritten for the instant the reaction starts, denoting the initial rate as r_0 and the concentrations of A and B_2 as $C_{A,0}$ and $C_{B_2,0}$, respectively:

dx.doi.org/10.1021/jp3093644 | J. Phys. Chem. B 2013, 117, 602−614

$$r_0 = k_f C_{A,0}^{\eta} C_{B_2,0}^{\xi} \quad \text{(A.4)}$$

Taking two different sets of initial concentrations, I and II, one may divide eq A.4 by itself to obtain

$$\frac{[r_0]_I}{[r_0]_{II}} = \frac{([C_{A,0}]_I)^{\eta}([C_{B_2,0}]_I)^{\xi}}{([C_{A,0}]_{II})^{\eta}([C_{B_2,0}]_{II})^{\xi}} \quad \text{(A.5)}$$

Therefore, in order to determine η and ξ, one simply performs a series of three sets of simulations with varying initial concentrations of A and B_2, as shown in Table 1.

Table 1. Method of Initial Rates for Noncatalytic Reaction Mechanism[a]

trial	$C_{A,0}$	$C_{B_2,0}$	r_0 [molecules/$n^2\tau$]
1	144	144	1.31×10^{-3}
2	72	144	6.84×10^{-4}
3	144	72	6.54×10^{-4}

[a] $\beta E_f = 10$, $n = 36$, and $\varphi = 1/3$.

During each of these particular simulations only the noncatalytic reaction was allowed to occur, with all other reactions turned off. Each simulation was repeated 1000 times, and the time trajectory of the concentration of A, C_A vs t, was averaged over all runs to obtain a smooth curve. The values of r_0 were obtained by plotting the averaged C_A vs t and taking the limiting slope of dC_A/dt at early time ($r_0 = -[\,dC_A/dt]_0 = -\lim_{t\to 0}\{dC_A/dt\}$).

Applying eq A.5 to trials 1 and 2 (note $[C_{B_2,0}]_I = [C_{B_2,0}]_{II}$), one obtains

$$\frac{[r_0]_1}{[r_0]_2} = \left(\frac{[C_{A,0}]_1}{[C_{A,0}]_2}\right)^{\eta} \quad \text{(A.6)}$$

Substituting the appropriate numbers and solving, $\eta = 0.94 \approx 1$. Similarly, with trials 1 and 3 one obtains $\xi = 1.00... \approx 1$. Therefore, the overall reaction order is $\eta + \xi = 2$, and the noncatalytic reaction is second order as implied by its molecularity. Equivalent simulation schemes were performed for the autocatalytic reaction, whereby it was confirmed that reaction is indeed third order.

AUTHOR INFORMATION

Corresponding Author

*E-mail: pdebene@princeton.edu. Tel.: (609) 258-5480.

Notes

The authors declare no competing financial interest.

ACKNOWLEDGMENTS

P.G.D. gratefully acknowledges the support of the National Science Foundation (NSF) (Grant CHE-1213343).

REFERENCES

(1) Khoury, G. A.; Baliban, R. C.; Floudas, C. A. *Sci. Rep.* **2011**, *1*, No. 90, DOI: 10.1038/srep00090.

(2) Klussmann, M.; Iwamura, H.; Mathew, S. P.; Wells, D. H.; Pandya, U.; Armstrong, A.; Blackmond, D. G. *Nature* **2006**, *441* (7093), 621−623.

(3) Breslow, R.; Levine, M. S. *Proc. Natl. Acad. Sci. U.S.A.* **2006**, *103* (35), 12979−12980.

(4) Lombardo, T. G.; Stillinger, F. H.; Debenedetti, P. G. *Proc. Natl. Acad. Sci. U.S.A.* **2009**, *106* (36), 15131−15135.

(5) Blackmond, D. G.; Klussmann, M. *Chem. Commun.* **2007**, *39*, 3990−3996.

(6) Klussmann, M.; White, A.; Armstrong, A.; Blackmond, D. *Angew. Chem., Int. Ed.* **2006**, *45* (47), 7985−7989.

(7) Klussmann, M.; Izumi, T.; White, A. J. P.; Armstrong, A.; Blackmond, D. G. *J. Am. Chem. Soc.* **2007**, *129* (24), 7657−7660.

(8) Kondepudi, D. K.; Kaufman, R. J.; Singh, N. *Science* **1990**, *250* (4983), 975−976.

(9) Kondepudi, D. K.; Bullock, K. L.; Digits, J. A.; Hall, J. K.; Miller, J. M. *J. Am. Chem. Soc.* **1993**, *115* (22), 10211−10216.

(10) Kondepudi, D. K.; Bullock, K. L.; Digits, J. A.; Yarborough, P. D. *J. Am. Chem. Soc.* **1995**, *117* (1), 401−404.

(11) Kondepudi, D. K.; Laudadio, J.; Asakura, K. *J. Am. Chem. Soc.* **1999**, *121* (7), 1448−1451.

(12) Viedma, C. *Phys. Rev. Lett.* **2005**, *94*, 6.

(13) Noorduin, W. L.; Izumi, T.; Millemaggi, A.; Leeman, M.; Meekes, H.; Van Enckevort, W. J. P.; Kellogg, R. M.; Kaptein, B.; Vlieg, E.; Blackmond, D. G. *J. Am. Chem. Soc.* **2008**, *130* (4), 1158−1159.

(14) Viedma, C.; Ortiz, J. E.; de Torres, T.; Izumi, T.; Blackmond, D. G. *J. Am. Chem. Soc.* **2008**, *130* (46), 15274−15275.

(15) Iggland, M.; Mazzotti, M. *Cryst. Growth Des.* **2011**, *11* (10), 4611−4622.

(16) Skrdla, P. J. *Cryst. Growth Des.* **2011**, *11* (5), 1957−1965.

(17) Hein, J. E.; Cao, B. H.; Viedma, C.; Kellogg, R. M.; Blackmond, D. G. *J. Am. Chem. Soc.* **2012**, *134*, 12629−12636.

(18) Frank, F. C. *Biochim. Biophys. Acta* **1953**, *11* (4), 459−463.

(19) Green, M. M.; Garetz, B. A. *Tetrahedron Lett.* **1984**, *25* (27), 2831−2834.

(20) Joyce, G. F.; Visser, G. M.; Vanboeckel, C. A. A.; Vanboom, J. H.; Orgel, L. E.; Vanwestrenen, J. *Nature* **1984**, *310* (5978), 602−604.

(21) Bolli, M.; Micura, R.; Eschenmoser, A. *Chem. Biol.* **1997**, *4* (4), 309−320.

(22) Sandars, P. G. H. *Origins Life Evol. Biospheres* **2003**, *33* (6), 575−587.

(23) Urata, H.; Aono, C.; Ohmoto, N.; Shimamoto, Y.; Kobayashi, Y.; Akagi, M. *Chem. Lett.* **2001**, *4*, 324−325.

(24) Ferris, J. P. *Philos. Trans. R. Soc., B* **2006**, *361* (1474), 1777−1786.

(25) Ernst, K. H. *Origins Life Evol. Biospheres* **2010**, *40* (1), 41−50.

(26) Mason, S. F.; Tranter, G. E. *Mol. Phys.* **1984**, *53* (5), 1091−1111.

(27) Mason, S. F.; Tranter, G. E. *Proc. R. Soc. London, A* **1985**, *397* (1812), 45−65.

(28) Kondepudi, D. K.; Nelson, G. W. *Nature* **1985**, *314* (6010), 438−441.

(29) Quack, M.; Stohner, J. *Chirality* **2001**, *13* (10), 745−753.

(30) Lente, G. *Phys. Chem. Chem. Phys.* **2007**, *9* (46), 6134−6141.

(31) Blackmond, D. G. *Cold Spring Harbor Perspect. Biol.* **2010**, *2* (5), a002147.

(32) Brandenburg, A.; Multamaki, T. *Int. J. Astrobiol.* **2004**, *3* (3), 209−219.

(33) Brandenburg, A.; Andersen, A.; Hofner, S.; Nilsson, M. *Origins Life Evol. Biospheres* **2005**, *35* (3), 225−241.

(34) Kondepudi, D. K.; Nelson, G. W. *Physica A* **1984**, *125* (2−3), 465−496.

(35) Hein, J. E.; Tse, E.; Blackmond, D. G. *Nat. Chem.* **2011**, *3* (9), 704−706.

(36) Budin, I.; Szostak, J. W. *Annu. Rev. Biophys.* **2010**, *39*, 245−263.

(37) Soai, K.; Shibata, T.; Morioka, H.; Choji, K. *Nature* **1995**, *378*, 767−768.

(38) Shibata, T.; Morioka, H.; Hayase, T.; Choji, K.; Soai, K. *J. Am. Chem. Soc.* **1996**, *118* (2), 471−472.

(39) Soai, K.; Sato, I.; Shibata, T.; Komiya, S.; Hayashi, M.; Matsueda, Y.; Imamura, H.; Hayase, T.; Morioka, H.; Tabira, H.; Yamamoto, J.; Kowata, Y. *Tetrahedron: Asymmetry* **2003**, *14* (2), 185−188.

(40) Blackmond, D. G.; McMillan, C. R.; Ramdeehul, S.; Schorm, A.; Brown, J. M. *J. Am. Chem. Soc.* **2001**, *123* (41), 10103−10104.

(41) Tolman, R. C. *Proc. Natl. Acad. Sci. U.S.A.* **1925**, *11*, 436−439.
(42) Kondepudi, D. K.; Kapcha, L. *Chirality* **2008**, *20* (3−4), 524−528.
(43) Blackmond, D. G.; Matar, O. K. *J. Phys. Chem. B* **2008**, *112* (16), 5098−5104.
(44) Fogler, H. *Elements of Chemical Reaction Engineering*; Prentice Hall: Upper Saddle River, NJ, 2008; Vol. *4*.
(45) Darwin, C. *The Life and Letters of Charles Darwin, Including an Autobiographical Chapter*; John Murray: London, 1887; Vol. *3*.
(46) Saito, Y.; Hyuga, H. *J. Phys. Soc. Jpn.* **2004**, *73* (7), 1685−1688.
(47) Mauksch, M.; Tsogoeva, S. B.; Wei, S. W.; Martynova, I. M. *Chirality* **2007**, *19* (10), 816−825.
(48) Blackmond, D. G. *Chirality* **2009**, *21* (3), 359−362.
(49) Mauksch, M.; Tsogoeva, S. B. *ChemPhysChem* **2008**, *9* (16), 2359−2371.
(50) Mauksch, M.; Wei, S. W.; Freund, M.; Zamfir, A.; Tsogoeva, S. B. *Origins Life Evol. Biospheres* **2010**, *40* (1), 79−91.
(51) Hatch, H. W.; Stillinger, F. H.; Debenedetti, P. G. *J. Chem. Phys.* **2010**, *133* (22), 224502.
(52) IUPAC Gold Book. http://goldbook.iupac.org/.
(53) Kang, H. C.; Weinberg, W. H. *J. Chem. Phys.* **1989**, *90* (5), 2824−2830.
(54) Kang, H. C.; Weinberg, W. H. *Acc. Chem. Res.* **1992**, *25* (6), 253−259.
(55) Blackmond, D. G. *Adv. Synth. Catal.* **2002**, *344* (2), 156−158.
(56) Butt, J. *Reaction Kinetics and Reactor Design*; Prentice Hall: Upper Saddle River, NJ, 1980.
(57) Espenson, J. *Chemical Kinetics and Reaction Mechanisms*; McGraw-Hill: New York, 1981.
(58) McKee, C.; Mortimer, M. *Chemical Kinetics and Mechanism*; The Royal Society of Chemistry: Cambridge, U.K., 2002.